CHAPTER 3

Design of molecular aptamer beacons for ATP-triggered cargo release

Part of this chapter was published: L. Cozzoli, L. Gjonaj, M. C. A. Stuart, B. Poolman, G. Roelfes, *Chem. Commun.* 2018, *54*, 260–263.

ABSTRACT

In this chapter, the previously discussed design of DNA G-quadruplex micelles was further investigated to obtain cargo release triggered by a small molecule. The ATP-binding aptamer was engineered to assume a hairpin conformation, with the stem region partially complementary to the micelles oligonucleotide headgroup. The formation of the aptamer-target complex induces a conformational change in the hairpin structure that promotes the hybridization of the complementary strands, thus leading to cargo release. The rational optimization of the molecular aptamer beacon design that led to the intended responsive system is discussed.

3.1 Introduction

3.1.1 Molecular beacons

Simplicity of synthesis, biocompatibility and predictable self-assembly make nucleic acids unique templates for the development of novel nanodevices with various applications, such as biosensing, bioimaging and therapy. In particular engineering of DNA molecules has proven to be advantageous to construct molecular probes able to recognize target nucleic acids or other molecules, such as proteins and small molecules.[1]

Tyagi and Kramer[2] reported in 1996 the first examples of molecular beacons (MBs). MBs are precisely designed DNA hairpin structures that can recognize and report the presence of specific nucleic acids in solution. These probes are formed by a single-stranded oligonucleotide and their structure is characterized by three portions: the loop, the stem and the reporter molecules (Figure 1). The loop domain determines the MB specificity, since it contains the target-binding region and its length ranges from 15 to 30 nucleotides. The stem region is formed by two short complementary sequences and it functions as a 'lock' to maintain the MB hairpin structure closed in the absence of a target. The reporter generally consists of a fluorophore and a quencher, attached to the opposite ends of the MB. In the absence of the target, the stem locks the MB structure and the fluorescence is quenched, due to the close proximity of the two dyes. Upon hybridization with the target DNA or RNA molecule, the hairpin opens and fluorescence is turned on.

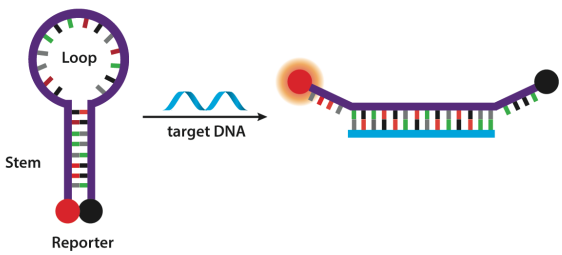

Figure 1. Schematic representation of the structure and recognition mechanism of a molecular beacon.

MBs are characterized by high selectivity and specificity and allow for real-time detection of nucleic acids. For these reasons, MBs are widely employed in biosensing, bioimaging and therapy.[1,3–6]

The loop region of MBs is responsible for its recognition properties. By incorporating an aptamer sequence in this region, the targets scope can be expanded from nucleic acids to small molecules or proteins. Aptamers are single-stranded oligonucleotides that bind to a target molecule with high affinity and selectivity. The aptamer sequence is generally isolated from an *in vitro* selection process called systematic evolution of ligands by exponential enrichment (SELEX).[7,8] This technique uses large combinatorial libraries of oligonucleotides, which are exposed to the target ligand, such as a protein or a small molecule. After iterative cycles of selection and amplification, only the sequence that binds to the target with higher affinity is isolated.

Molecular aptamer beacons (MAB) combine the mechanism of signal transduction typical of MBs with the binding specificity of aptamers.[9,10] The aptamer can be incorporated into the classical stem-loop structure, however for some aptamers the constricted conformation determines a decrease in the binding affinity. A different approach is based on the functionalization of the aptamer with the reporter molecules, without requiring the formation of the hairpin structure. The binding of the aptamer with the target molecule often determines conformational rearrangements in its secondary structure, which can be transduced in changes in the fluorescence signal. Several aptamer-based sensors have been developed for the detection of a wide range of molecules, such as drugs, proteins or other organic or inorganic molecules. [11–14]

Fluorophore-labeled MBs present some drawbacks related to the high costs of DNA labeling and limited availability of the probes. Additionally, the binding affinity towards the target can be decreased due to the chemical modification of the scaffold. Therefore, to overcome these problems 'label-free' strategies have been developed. A widely used strategy is based on the combination of MBs with G-quadruplex DNAzymes.[15–18] Teller *et al.* designed an aptamer-DNAzyme hairpin for the

colorimetric detection of a small molecule (adenosine monophosphate, AMP) or a protein (lysozyme).[19] The MAB consisted of an aptamer sequence attached to horseradish peroxidase (HRP)-mimicking DNAzyme sequence. In the absence of the analyte the scaffold assumes a stem-loop structure, preventing the folding of the DNAzyme into its active conformation. The binding of the aptamer with its target results in the uncaging of the DNAzyme from the stem region and generates the colorimetric readout (Figure 2a).

3.1.2 DNA-based ATP sensing

Adenosine triphosphate (ATP) also referred as the 'molecular unit of currency' of intracellular energy transfer, plays a critical role in the regulation of cellular metabolism.[20] The detection of ATP is highly important for biochemical purposes and for clinic diagnosis.

The ATP-binding aptamer (ABA) is a 27-mer oligonucleotide and binds to ATP with a K_d of ~ 6 μM and with a similar affinity to AMP and adenosine.[21] Upon target binding, the structure of ABA switches from a single stranded conformation into a G-quadruplex (G-4) formed by two stacked G-quartets and two flanked double-helix stems. The proposed binding site for ATP is located between two adenosine residues adjacent to the upper G-quartet (Figure 2b). ABA is extensively employed in the design of DNA-based sensors for ATP.[22]

Even if several signaling strategies, based on colorimetry[23,24] or electrochemistry[25–27], have been developed, fluorescence signaling remains the preferred approach because of its simplicity and the large selection of available dyes that can be readily attached to DNA. However, labeling of the aptamer with fluorescent dyes may lead to a significant loss in their affinity and specificity. For this reason, alternative strategies are employed, requiring labeling on a second DNA strand which interacts with ABA and acts as a fluorescence reporter of its conformational changes upon ATP binding.[14,28] Additionally, 'label-free' ABA-sensors have been developed, which employ photoactive compounds or intercalating dyes to detect the binding between the aptamer and ATP.[29–31] Recently, Wang *et*

al. reported a label-free approach using Thioflavin T (ThT) for the detection of ATP.[32] ThT is a fluorescent ligand of ABA but with lower affinity (K_d ~ 89 μM) compared to ATP. The addition of ATP generates a conformational change in the structure of ABA, reducing the interaction with ThT and leading to a decrease in its fluorescence emission (Figure 2c).

The development of novel ATP-sensing system is of particular interest for the detection of intracellular levels of ATP, cell imaging or drug delivery. However the use of MB-based nucleic acids probes in vivo is challenging due to inefficient cell internalization and oligonucleotide degradation. Generally, functionalization of gold nanoparticles (AuNPs) with oligonucleotides is the strategy used to enhance stability and cellular uptake, but it is limited by their cytotoxicity at high concentrations.[33–35] Özalp *et al.* designed an ATP-responsive MAB on the surface of mesoporous nanoparticles as nanovalves for drug delivery.[36] In the presence of ATP, the aptamer hairpin switches its conformation from duplex to single stranded DNA in the region of the molecule close to the surface. Due do the different thickness of the two conformations, the guest molecules are released selectively upon target binding (Figure 2d).

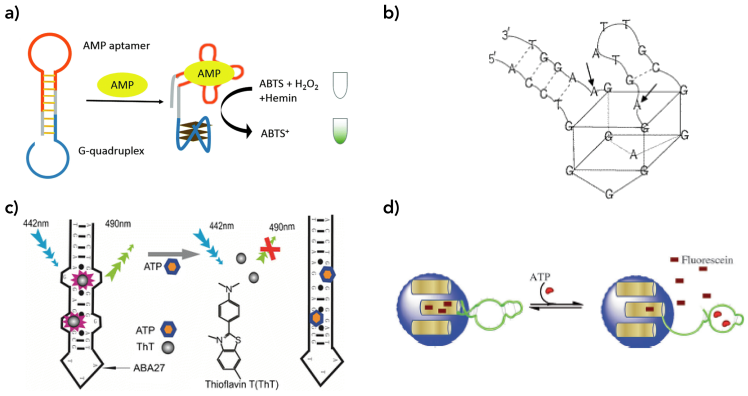

Figure 2. (a) Aptamer-DNAzyme hairpin for the colorimetric detection of AMP.[19] Picture adapted from ref.1 with permission. **(b)** Structure of the ATP aptamer. The arrows indicates the binding regions of ATP.[21] Picture adapted from ref. 22 with permission. **(c)** The principle of ThT for label-free aptamer-based ATP detection. Picture adapted from ref. 32 with permission. **(d)** Aptamer-capped mesoporous silica nanoparticles for ATP-triggered drug delivery. Picture adapted from ref. 36 with permission.

3.2 Aim

In this study, we aimed to develop a DNA-based system responsive to ATP. In the previous study, discussed in Chapter 2, DNA G-4 micelles were designed and we showed that the G-4 motif plays an important role in their stability. Cargo release was obtained by hybridization of the oligonucleotide headgroup with its complementary strand. Based on these findings, a similar design was employed in combination with a structure-switching DNA aptamer as the DNA exchange strand, to achieve selective cargo release in the presence of ATP.

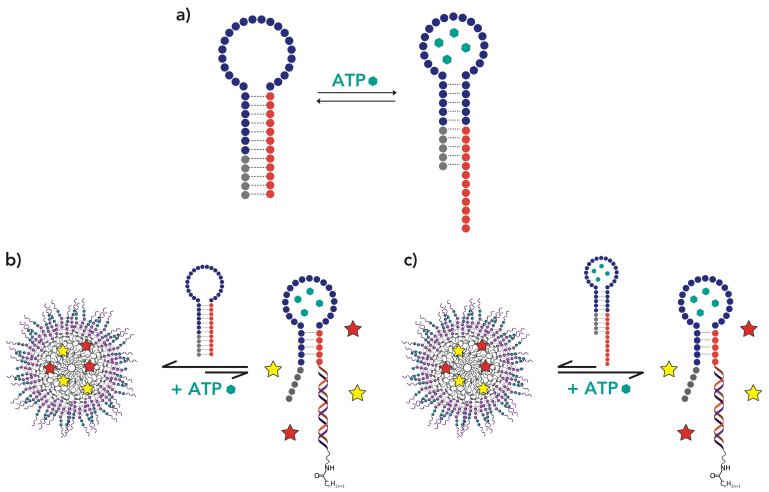

Figure 3. (a) Design of the DNA hairpin composed of the ATP-binding domain (in blue) and the responsive domain (in red). An extra sequence (regulation domain, in grey) is added to modulate the equilibrium between the two conformations. **(b)** In the absence of ATP, the responsive domain is locked and the interaction with the complementary strand in the G-4 micelles is disfavored. **(c)** When ATP binds to the recognition domain, the structure of the hairpin rearranges, exposing the responsive domain. This promotes the hybridization of the responsive domain with its complementary strand, leading to micelle disruption and release of the cargo.

3.3 Design

The proposed strategy to achieve selective cargo release in the presence of ATP envisages the employment of the ATP-binding aptamer,

accurately engineered to assume a hairpin structure that can change its conformation upon ligand binding. The hairpin is composed of: (a) the ATP-recognition domain; (b) the responsive domain, that interacts with the DNA headgroup of the micelles; and (c) the regulation domain that modulates the equilibrium between the two conformations of the hairpin. In the absence of ATP, the hairpin is preferentially in a locked conformation that inhibits the responsive domain to interact with the G-4 micelles. Conversely, upon binding of ATP the hairpin structure is rearranged, liberating the responsive domain, which can hybridize with the G-4 micelles, leading to cargo release (Figure 3)

3.4 Results and discussion

Three different designs of MABs were investigated. The oligonucleotide sequences of the MABs employed in each design are reported in Table 1.

3.4.1 First design

In our first design, we constructed the ATP aptamer hairpin by lenghtening the original sequence on both the 5'and 3'termini. Specifically, a complementary sequence to the headgroup of the G-4 micelles was appended on the 3'end (responsive domain), while an extra strand was attached to the 5'end (regulation domain). The complementary sequence represents the responsive domain of the hairpin, being responsible of the hybridization with the G-4 micelles and subsequently allowing the release of the dye. The regulation domain was designed to maintain the conformation of the hairpin locked before the addition of ATP, due to its hybridization with part of the responsive domain. One of the main prerequisite in designing such a system is that the duplex in the hairpin stem needs to be more stable than the duplex formed by the responsive domain and its complement maintaining the hairpin structure closed in absence of the ligand. Neverthless, it should still allow the conformational change of the aptamer and the hybridization with the

micelles headgroup upon ligand binding. This would result in the selective dye release in the presence of ATP.

Table 1. Oligonucleotide sequences used in the MAB design. The ATP-binding domain is indicated in bold; the responsive domain is underlined and mismatches on the regulation domain are indicated in italic.

Name	Sequence (5′-3′)
First design: lipid-G-4 micelles $C_{18:1}$-OL1 ($C_{18:1}$- GGGTTTAAGTGTAGTTAA)	
ABA-1	AG*C*GTA*A*TTA*T*GAACCT**TCCTGGGGGAGTATTGCGGAGGAAGGT**TCT TAACTACACTTAAACCC
ABA-2	AG*C*GTA*A*TTAAGAA*T*CT**TCCTGGGGGAGTATTGCGGAGGAAGGT**TCT TAACTACACTTAAACCC
Second design: lipid-G-4 micelles $C_{18:1}$-OL2 ($C_{18:1}$- GGGTTCACCTGGA)	
ABA-3	G*T*GTGC**ACCTGGGGGAGTATTGCGGAGGAAGGT**TCCAGGTG*T*ACCC
ABA-4	GTC**ACCTGGGGGAGTATTGCGGAGGAAGGT**TCCAGGTGACCCC
ABA-5	TGC**ACCTGGGGGAGTATTGCGGAGGAAGGT**TCCAGGTG*C*ACCC
Third design: lipid-G-4 micelles $C_{18:1}$-OL2 ($C_{18:1}$- GGGTTCACCTGGA)	
ABA-6	C**ACCTGGGGGAGTATTGCGGAGGAAGGT**TCCAGGTGAACCC
ABA-7	C**ACCTGGGGGAGTATTGCGGAGGAAGGT**TCCAGG*A*GAACCC
ABA-8	C**ACCTGGGGGAGTATTGCGGAGGAAGGT**TCCAGGTG*T*ACCC

Initially, two similar designs (ABA-1 and ABA-2) were studied, both 65-mers. The responsive domain is formed in both cases by a 18-mer perfectly complementary to the oligonucleotide headgroup of the micelles. To decrease the energy gap between the closed and the open conformation of the hairpin, we introduced 3 mismatches in the regulation domain for both ABA-1 and ABA-2 (Figure 4 and Table 1 for the sequences).

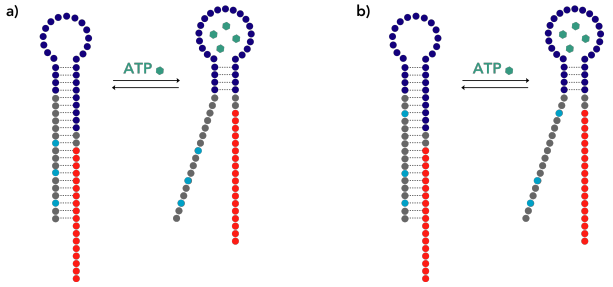

Figure 4. Schematic representation of the first design MABs **(a)** ABA-1 and **(b)** ABA-2. The pale blue dots indicate the position of the mismatches in the regulation domain.

The designed MABs were tested using native polyacrylamide gel electrophoresis (Figure 5a) to study the destabilization of the G-4 micelles in the presence of ATP. ABA-1 was incubated with the preformed G-4 micelles of $C_{18:1}$-OL1, showing no micelle destabilization in the absence of ATP (lane 3). In fact, the upper band, corresponding to the G-4 micelle in the gel, didn't display any change. The same was observed when 5 mM ATP were added to the solution of ABA-1 and $C_{18:1}$-OL1 (lane 5), indicating that the G-4 micelles are still stable under these conditions.

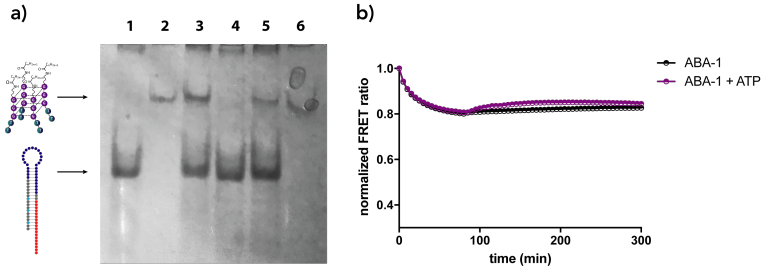

Figure 5. (a) Monitoring the destabilization of the G-4 using native 10% polyacrylamide gel electrophoresis. Lane 1: ABA-1; lane 2: $C_{18:1}$-OL1; lane 3: $C_{18:1}$-OL1 + ABA-1; lane 4: ABA-1 + ATP; lane 5: ABA-1 + ATP + $C_{18:1}$-OL1; lane 6: $C_{18:1}$-OL1 + ATP. **(b)** Normalized FRET ratio of the G-4 micelles in presence of ABA-1 alone (dark) or upon addition of 5 mM ATP (purple).

To confirm these results, the release of hydrophobic probes from the core of the micelles over time was monitored by measuring Förster resonance energy transfer (FRET) efficiency. The FRET pair that was chosen consisted of 3,3'-dioctadecyloxacarbocyanine perchlorate (DiO, donor) and 1,1'-dioctadecyl-3,3,3',3'-tetramethylindocarbocyanine perchlorate

(DiI, acceptor). When both dyes are encapsulated in one micelle, excitation at 450 nm (excitation of the donor) will result in energy transfer due to their close proximity, leading to fluorescence emission at 575 nm (emission of the acceptor). In contrast, when the micelles disassemble, the two dyes are released and a decrease in the FRET efficiency should be observed. The fluorescence experiments were performed on samples of $C_{18:1}$-OL1 dissolved in a solution of bovine serum albumin (BSA) in PBS (45 mg/mL), pH 8.5 at 37 ˚C with λ_{ex} 450 nm, monitoring the emission in the range of 465-700 nm. A pH of 8.5 was employed for this study, due to the described interaction between BSA and ATP at lower pH.[37,38] During a typical experiment, the micelles fluorescence was monitored for 80 min before the addition of the MAB/MAB-ATP complex (Figure 5b).

The FRET ratio did not display any significant change upon addition of ABA-1 and ATP, indicating that the dyes are not released from the hydrophobic core of the micelles. These results confirm that the DNA G-4 micelles are not destabilized by the MAB, even in the presence of ATP. Similar results were obtained for ABA-2 (data not shown), indicating that none of the proposed designs are suitable for our purpose. A possible explanation for the results is most likely related to the decrease in affinity between the recognition sequence of the aptamer and the ATP. In fact, the increase in the overall length of the scaffold containing the aptamer sequence can lead to reduced binding with the target molecule. Moreover, the stems of the designed MABs are long and presumably the interactions between the two strands are too strong, which does not favor the conformational rearrangement of the hairpin.

Thioflavin T (ThT) is a fluorescent ligand for ABA, used for sensing the binding of the aptamer with ATP (Figure 2c).[32] The binding of ATP to ABA results in a decrease of the fluorescence emission of ThT, due to the reduced interaction of the aptamer with the fluorescent ligand. The fluorescence emission of ThT was measured after incubation with ABA-1 and changes were detected upon addition of 5 mM ATP. As can be observed in Figure 6c, the native ATP-binding aptamer ABA promotes the fluorescence emission of ThT, but upon addition of ATP a dramatic

decrease of the fluorescence intensity is observed. The same experiment was performed for ABA-1 and ABA-2, resulting only in a modest decrease in fluorescence in the presence of the target molecule. These results evidence that the binding affinity between the aptamer and its ligand is reduced in the new constructs. This is most likely caused by the strong interaction between the two strands in the stem region that hinders the rearrangement of the aptamer to the active conformation for the binding to ATP.

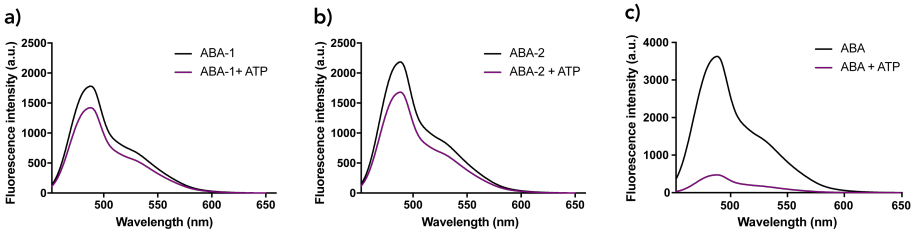

Figure 6. Fluorescence emission spectra of ThT complexed with **(a)** ABA-1 **(b)** ABA-2 **(c)** ABA (dark) and upon addition of 5 mM ATP (purple). A significant decrease in fluorescence emission is observed mainly in the case of ABA, indicating high affinity between the aptamer and ATP.

The outcomes of the performed experiments indicate that the proposed scaffolds are not suitable for achieving ATP-triggered cargo release.

3.4.2 Second design

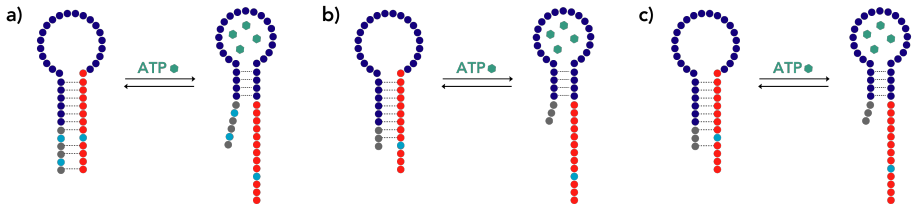

Figure 7. Schematic representation of the MABs **(a)** ABA-3, **(b)** ABA-4 and **(c)** ABA-5. The pale blue dots indicate the position of the mismatches.

The obtained results pointed out that the MAB scaffold should contain as little modifications as possible on the aptamer sequence, in order to reduce the detrimental effects on the aptamer binding affinity. Thus, two

new designs of the ATP-responsive MAB were conceived, decreasing the overall length of the scaffold from a 64-mer to a 46-mer (ABA-3) and a 43-mer (ABA-4 and ABA-5) respectively. Özalp *et al.*[36] employed a similar scaffold, which they incorporated on a nanomaterial as a nanovalve for drug delivery.

Both the optimized designs consisted of the aptamer-binding sequence attached directly to the responsive domain on the 3'terminus (Table 1). The length of both the responsive domain and the regulation domain was reduced compared to the previous design. Specifically, the complementary sequence consisted of a 13-mer, while the regulation domain was significantly shortened to six nucleobases for ABA-3 and to three nucleobases for ABA-4 and ABA-5. Two mismatches were introduced in the regulation domain of ABA-3, to further destabilize the interaction of the duplex in the hairpin stem and promote the rearrangement in the presence of ATP. Moreover, in all the designs, a mismatch was introduced on the responsive domain, to decrease the possibility of the hairpin rearrangement in the absence of the target molecule.

As for the previous design, studies on the destabilization of the G-4 micelles formed by $C_{18:1}$-OL2 were performed by native polyacrylamide gel electrophoresis and fluorescence (Figure 8). However, the experiments led to negative outcomes for the three scaffolds tested, indicating that the G-4 micelles are not destabilized upon addition of ATP. Specifically, the band corresponding to the G-4 micelles is still visible with the same retention in the gels, even in presence of both the MAB and ATP (lane 5). In addition, the fluorescence experiment indicates that the dyes incorporated in the micelles are not released upon addition of ATP, since the FRET ratio is stable.

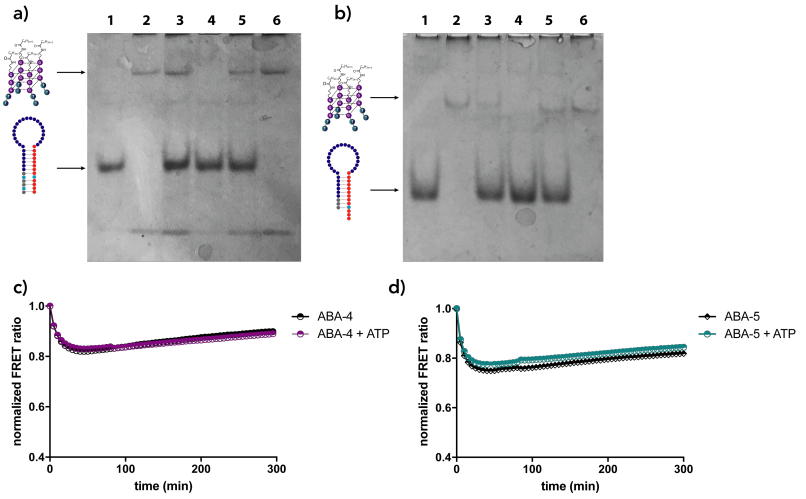

Figure 8. Monitoring the destabilization of the G-4 using native 10% polyacrylamide gel electrophoresis **(a)** ABA-3 and **(b)** ABA-5. Lane 1: MAB; lane 2: $C_{18:1}$-OL2; lane 3: $C_{18:1}$-OL2 + MAB; lane 4: MAB + ATP; lane 5: MAB + ATP + $C_{18:1}$-OL2; lane 6: $C_{18:1}$-OL2 + ATP. **(c)** FRET experiment to measure the ATP-triggered cargo release performed with ABA-4 and **(d)** ABA-5. Similar results were obtained with ABA-3.

To gain further information about the affinity of the MABs for the target molecule, the fluorescence emission of ThT was measured with and without ATP (Figure 9). Both ABA-4 and ABA-5 did not show a significant decrease in the fluorescence emission of ThT upon addition of ATP, most likely indicating a reduced affinity between the aptamer and its ligand due to modifications on the scaffold. Interestingly, the fluorescence emission of ThT complexed with ABA-3 undergoes a 4-fold reduction in presence of ATP. This result shows that the aptamer retains some of its affinity towards ATP, despite of the lengthening of the recognition sequence. Nevertheless, this scaffold did not produce any destabilization of the G-4 micelles. The presence of a mismatch on the responsive domain could give rise to a reduced interaction with the oligonucleotide headgroup of the micelle, therefore preventing the G-4 disruption. More studies are necessary to confirm the effects of a single mismatch on the thermodynamics of the system.

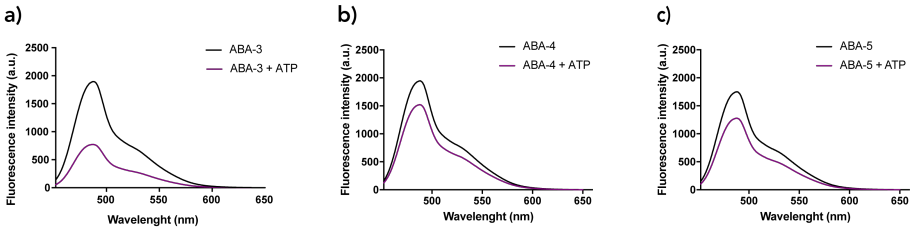

Figure 9. Fluorescence emission spectra of ThT complexed with **(a)** ABA-3 **(b)** ABA-4 **(c)** ABA-5 (dark) and upon addition of 5 mM ATP (purple).

3.4.3 Third design

Based on the previous results, we optimized the MAB design to contain only the two essential regions of the scaffold: the recognition domain and the responsive domain. A single nucleobase is incorporated as modulation domain, which interacts with its complement only in the closed conformation of the hairpin. A new MAB scaffold was proposed (ABA-6) and two analogues containing mismatches (ABA-7 and ABA-8) were also investigated (Figure 10, Table 1 for the oligonucleotide sequences).

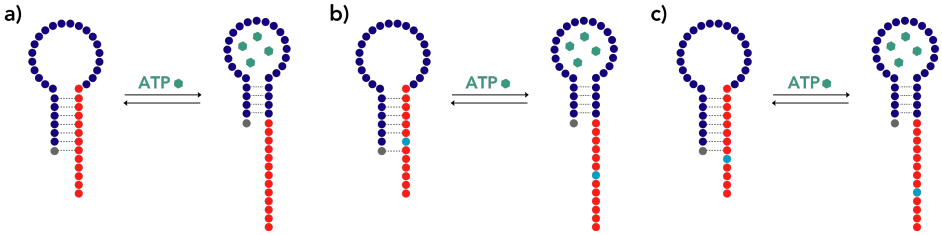

Figure 10. Schematic representation of the MABs **(a)** ABA-6 and **(b)** ABA-7 and **(c)** ABA-8. The pale blue dots indicate the position of the mismatches.

Specifically, ABA-7 is characterized by a mutated nucleobase on the responsive domain, that is a mismatch for both the single strand in the hairpin stem and the oligonucleotide headgroup of the G-4 micelles. Conversely, ABA-8 has a mismatch at the end of the responsive domain that affects only its interaction with the G-4 micelle headgroup.

The proposed MABs scaffolds were investigated first by native polyacrylamide gel electrophoresis (Figure 11). Both ABA-7 and ABA-8 did not give any destabilization of the G-4 micelles, since the corresponding band was still visible in the presence of ATP (lane 5). Differently, in the case of ABA-6 the gel indicated that the micelles are destabilized when

incubated with both the MAB and ATP (lane 5). In fact, the band corresponding to ABA-6 became less intense and a new band with lower retention appeared, suggesting that the hybridization between the MAB responsive domain and its complementary strand took place. The same band is also visible when ABA-6 and the G-4 micelles were incubated together in the absence of ATP (lane 3), indicating that the destabilization of the micelles is presumably occurring under these conditions.

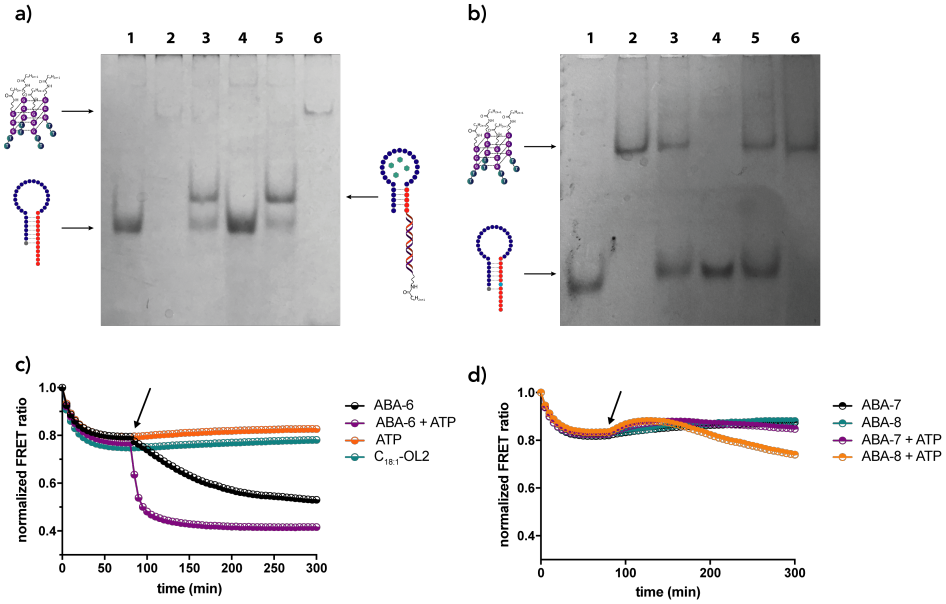

Figure 11. Monitoring the destabilization of the G-4 micelles using native 10% polyacrylamide gel electrophoresis **(a)** ABA-6 and **(b)** ABA-7. Similar results to ABA-7 were obtained for ABA-8. Lane 1: MAB; lane 2: $C_{18:1}$-OL2; lane 3: C18:1-OL2 + MAB; lane 4: MAB + ATP; lane 5: MAB + ATP + $C_{18:1}$-OL2; lane 6: $C_{18:1}$-OL2 + ATP. **(c)** FRET experiment to measure the ATP-triggered cargo release performed with ABA-6 and **(d)** ABA-7 and ABA-8. The arrow indicates the time point at which the addition was done.

The results obtained with ABA-6 indicate that this scaffold allows for the hairpin rearrangement to its open conformation. In order to quantify the G-4 micelles destabilization upon addition of ATP, we performed the FRET experiment with the G-4 micelles and the MABs. In the experiment with ABA-6, upon addition of ATP the micelles were immediately disrupted and the dyes were released (Figure 11c, purple). As already evidenced by the gel electrophoresis, destabilization of the micelles does

occur in the presence of ABA-6 without ATP but at a much slower rate and lower efficiency (Figure 11c, black). As control, ATP was added to the G-4 micelles in the absence of the MAB but this had no effect on the FRET ratio, indicating that the observed decrease is produced by the simultaneous presence of ABA-6 and ATP.

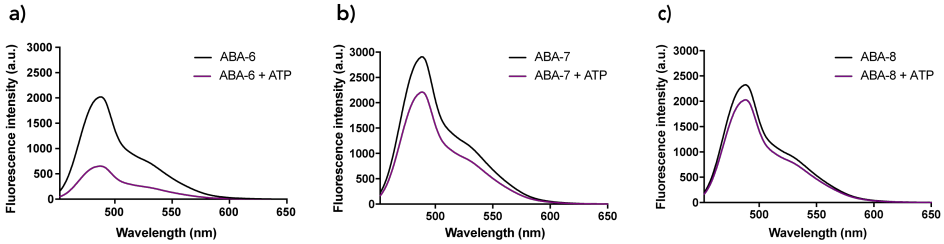

Figure 12. Fluorescence emission spectra of ThT complexed with **(a)** ABA-6 **(b)** ABA-7 **(c)** ABA-8 (black) and upon addition of 5 mM ATP (purple).

The same experiment was carried out for ABA-7 and ABA-8, confirming the results obtained by gel electrophoresis (Figure 11d). The micelles treated with ABA-8 and ATP showed only a small destabilization compared to the control experiment, therefore suggesting that the introduction of a mismatch in the scaffold influences drastically the equilibrium between closed and open conformation of the hairpin.

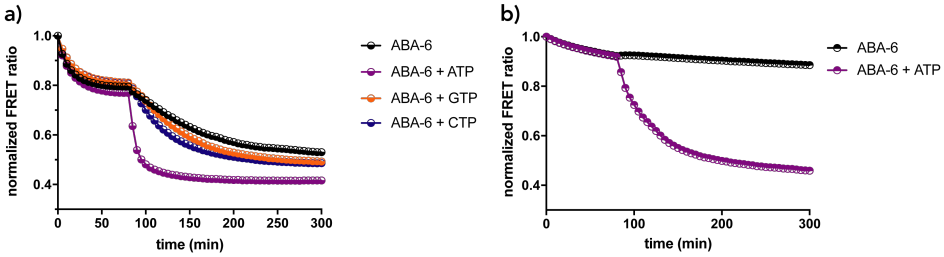

Figure 13. (a) Normalized FRET ratio over time measured for the DNA G-4 micelles responsive to ATP. In the presence of the MAB (ABA-6, black) the micelles are destabilized but at a slower rate than in the presence of 5mM ATP (purple). Upon addition of ATP, an immediate decrease of the FRET ratio is observed, indicating dye release. The response is specific for ATP, since the addition of GTP (orange) or CTP (blue) does not affect the stability of the micelles. **(b)** FRET experiment performed at 25 °C.

The affinity between the MABs and ATP was investigated using the ThT assay (Figure 12): ABA-6 showed a 4-fold reduction in the ThT

fluorescence emission in the presence of ATP, confirming that the ligand is still able to bind to the recognition sequence of the aptamer. The fluorescence emission was not altered significantly in the case of ABA-7 and ABA-8, presumably indicating that the assumed conformation of the hairpin prevents the interaction between the aptamer and its ligand.

The results obtained for ABA-6 demonstrate that this scaffold is suitable for achieving ATP-triggered cargo release. The FRET experiment proved that the destabilization of the G-4 micelles is faster and more efficient when ATP is added to the mixture. The selectivity for ATP was determined by performing the FRET experiment using two analogue nucleotides, guanosine-5'-triphosphate (GTP) and cytidine-5'-triphosphate (CTP). The results show that in this case the decrease in the FRET ratio is comparable to the system in absence of ATP, confirming that the system is selectively releasing the cargo in presence of ATP (Figure 13a).

To reduce the destabilization of the micelles in presence of the MAB alone, the FRET experiment was performed at lower temperature (25 °C). Figure 13b shows that the FRET ratio is stable under these conditions and in the absence of ATP (black). Upon addition of 5 mM ATP, the FRET ratio decreases with a slower kinetics compared to the experiment at 37 °C, but reaching the same value at the final time point of the experiment. Therefore, under these conditions, the DNA G-4 micelles are not destabilized by the MAB and the dye release takes place only in the presence of ATP.

3.5 Conclusions

In conclusion, this chapter describes the design optimization of MABs used in combination with DNA G-4 micelles to achieve ATP-triggered cargo release. Different strategies have been investigated toward this goal. Native polyacrylamide gel electrophoresis and fluorescence studies were performed on the proposed scaffolds. Unfortunately, both the first and second design of MABs did not lead to successful destabilization of the micelles in the presence of ATP. The lack of destabilization might be

caused by the decreased affinity of the aptamer recognition sequence for its ligand, as proved by the ThT assay. The lengthening of the aptamer could hinder the hairpin rearrangement from its closed to open conformation, therefore preventing the binding of ATP. Based on the results obtained, a rational optimization on the scaffold was carried out, by reducing the overall length of the MAB and increasing the flexibility of the hairpin.

The third design of MAB (ABA-6) proved to be a suitable scaffold for the intended goal. Fluorescence studies indicate that the DNA G-4 micelles are significantly destabilized in the presence of both the MAB and ATP, with higher efficiency and rate than in the absence of ATP. The system proved to be selective for ATP, since it was not responsive to similar nucleosides triphosphate, such as GTP or CTP. Upon addition of ATP the hairpin readily switched its conformation from closed to open, liberating the responsive domain and favoring its hybridization with the oligonucleotide headgroup of the micelles. However, the addition of ABA-6 alone promotes partially the opening of the hairpin, therefore leading to moderate micelle destabilization in the absence of ATP. To reduce this effect, the experiment was performed at lower temperature, resulting in negligible dye release prior to ATP addition.

The presence of mismatches on the scaffold of ABA-6 led to complete lack of response of the G-4 micelles. It is conceivable that the mismatches decrease the extent of hybridization between the responsive domain of the hairpin and the headgroup of the micelles, therefore resulting in negligible dye release. Moreover, a detrimental effect of the mismatches on the ATP-binding affinity was observed in the ThT assay.

In conclusion, a successful design of MAB for ATP-triggered cargo release from DNA G-4 micelles was developed. This DNA aptamer-based approach to G4-micelle disassembly is highly versatile and we envision its application to different targets or stimuli. Future studies are aimed to the optimization of the system in order to achieve micelle destabilization at lower concentrations of the trigger molecule. Nevertheless, the designed

MAB proved to be selective and efficient and holds great promises for the development of stimuli responsive DNA-based nanodevices.

3.6 Experimental section

3.6.1 General remarks

Chemicals were purchased from Sigma Aldrich or Acros and used without further purification. ^{1}H-NMR and ^{13}C-NMR spectra were recorded on a Varian 400 MHz in $CDCl_3$. Chemical shifts (δ) are denoted in ppm using residual solvent peaks as internal standard. Synthetic oligonucleotides were purchased from Biotez Berlin-Buch GmbH. Oligonucleotide concentrations were determined using Nanodrop 2000 (Thermo Fisher Scientific). Extinction coefficients of the oligonucleotides (ε_{260}) were calculated by Oligo Analyzer 3.1 from IDT (Integrated DNA Technologies). Reversed-phase HPLC (RP-HPLC) purifications were performed on a Shimadzu LC-10AD VP using a Xbridge Prep C8 column (10 x 150 mm, particle size 5 µm) from Waters Corporation. 0.1 mM triethylammonium acetate (TEAA) at pH=7.0 (solvent A) and acetonitrile (solvent B) were used as the mobile phase at a flow rate of 1 mL/min. Gradient: 5% B for 5 min, linear gradient to 90% B in 5 min, to 100% B in 10 min, isocratic for 5 min. Re-equilibration of the column at 5% B for 5 min. The column was heated to 65 ˚C. UPLC-MS on the conjugates was performed on an Acquity TOF Detector (ESI TOF- MS) coupled to Waters Acquity Ultra Performance LC using an Acquity BEH C4 (1.7 µm 2.1 x 150 mm). 15 mM TEAA at pH=7.2 (solvent A) and methanol (solvent B) were used as the mobile phase at a flow rate of 0.2 mL/min. Gradient: 95% A for 5 min, linear gradient to 5% A in 5 min. Re-equilibration of the column at 95% A for 4 min. The column was heated to 60 ˚C. The ESI ion source was operated in negative mode and mass spectra were collected between 200 and 3000 *m/z*. UPLC-MS chromatograms were analyzed with MassLynx V4.1. Circular dichroism (CD) and UV-visible spectra were recorded on Jasco J-815 Spectropolarimeter and Jasco V-660 Spectrophotometer, respectively. Fluorescence was recorded on a Jasco FP-8300 Spectrofluorometer.

3.6.2 Synthesis of the oleic acid *N*-hydroxysuccinimidic ester

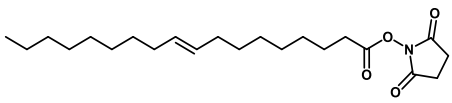

Oleic acid (3 mmol, 1 eq) and *N*-hydroxysuccinimide (3.3 mmol, 1.1 eq.) were dissolved in 20 mL dichloromethane, under N_2 atmosphere. Then EDC (1-ethyl-3-(3-dimethylaminopropyl) carbodiimide hydrochloride) (3.3 mmol, 1.1 eq) was added to the mixture in two portions. The reaction was stirred overnight. The mixture was extracted with H_2O (2 x 30 mL) and then washed with brine (2 x 30 mL). The organic layer was dried over $MgSO_4$ and the solvent was evaporated under reduced pressure. The residual solid was recrystallized from EtOH. The obtained residue was purified by flash column chromatography using dichloromethane as eluent (50%, transparent oil).

^{1}H NMR (400 MHz, $CDCl_3$) δ 0.88 (t, J = 6.8 Hz, 3H), 1.22 – 1.44 (m, 20 H), 1.74 (m, 2H), 1.97 – 2.06 (m, 4H), 2.60 (t, J = 7.5 Hz, 2H), 2.83 (d, J = 3.3 Hz, 4H), 5.29 – 5.40 (m, 2H).

3.6.3 Synthesis of the DNA-lipid conjugates

The amino-modified oligonucleotide was solubilized in 350 µL of 200 mM NaH_2PO_4 pH=8.5 (350 µM) and 250 µL of the alkyl *N*-hydroxysuccinimyl-ester in DMF (20 mg/mL) were added. The reaction was stirred overnight at 37°C or 70 °C when precipitation of the alkyl NHS-ester occurred. The functionalized DNA was purified by size exclusion chromatography (NAP-10, GE Healtcare) using triethylamine acetate (TEAA) buffer 50 mM pH=7.2. The lyophilized conjugates were subsequently purified by RP-HPLC and analyzed by UPLC-MS (TOF).

Table 2. ESI(-) of the synthesized DNA-lipid conjugates from UPLC-MS.

DNA-lipid conjugate	$MW_{observed}$	$MW_{calculated}$ (Da)	Rt (min)
$C_{18:1}$- GGGTTTAAGTGTAGTTAA	6002.9*	6010.2	8.6
$C_{18:1}$- GGGTTCACCTGGA	4389.3*	4392.2	8.4

*calculated from observed $[M-3H]^{3-}$ or $[M-4H]^{4-}$

3.6.4 Annealing procedure for the G-4 formation

The purified DNA-lipids were solubilized in 30 mM Tris-HCl, 80 mM KCl, pH=7.2 and then heated to 90˚C for 15 min. The solution was slowly cooled to room temperature and then stored at 4˚C overnight.

3.6.5 Native polyacrylamide electrophoresis (PAGE)

Electrophoresis experiments were performed according to standard procedures with 10% polyacrylamide gels (acrylamide-bis acrylamide 19:1, 40% w/v). 1 mM KCl was added to both the gel and the running buffer (1x TBE). The samples were prepared in 30 mM Tris-HCl, 80 mM KCl, 5 mM $MgCl_2$ pH= 8.5 and annealed beforehand. The oligonucleotides were mixed with the MABs and/or 5 mM ATP and incubated at 37 ˚C for 1h previous to loading. The final concentration loaded in the gel was 5 μM. The gel was run at 80 V for 1.5 h at 4 ˚C and stained with Stains-All (Sigma Aldrich).

3.6.6 Förster resonance energy transfer (FRET) experiment procedure

The two dyes 3,3′-dioctadecyloxacarbocyanine perchlorate (DiO) and 1,1′-dioctadecyl-3,3,3′,3′-tetramethylindocarbocyanine perchlorate (DiI), were suspendend in ethanol at 2 mg/mL. The DNA-lipid conjugates were also dissolved in ethanol and 5 wt % of each dye was added to the samples. The ethanol was evaporated in a vacuum concentrator, resulting in a thin lipid film. The film was rehydrated with 25 mM $NaHPO_4$, 50 mM KCl pH=8.5 to reach a final concentration of 1 mg/mL. The mixture was heated to 65 ˚C for 15 mins and then cooled slowly to room temperature. The sample was centrifuged in tube filters with a pore size of 0.45 μm to remove aggregates. For fluorescence experiments the samples were diluted in 90% bovine serum albumin (BSA) in PBS buffer (50 mg/ml in 15 mM $NaHPO_4$, 150 mM NaCl pH=8.5). The final concentration of the DNA-lipids was 15 μM. The fluorescence was measured in a quartz cuvette with 1.0 cm path length. The samples were excited at 450 nm and emission was measured from 465 nm to 700 nm for 5 hours at 37 ˚C. The MAB (1.2 eq) and/or ATP (final concentration 5 mM) were added after 80 mins and mixed by pipetting up and down. FRET efficiency was measured by calculating the FRET ratio ($I_{575}/(I_{575} + I_{510})$) at each time point to monitor micelle stability.

3.6.7 Thioflavin T (ThT) assay procedure

A stock solution of the MABs was prepared in PBS buffer (15 mM $NaHPO_4$, 150 mM NaCl pH=8.5), heated at 90 °C for 10 min, and gradually cooled to room temperature. The stock was diluted in Tris-HCl buffer (Tris-HCl 20 mM, NaCl 300 mM, $MgCl_2$ 5 mM pH 8.5) to reach a final concentration of 7 μM. Then, ThT (25 μM) and/or and ATP (5 mM) were mixed with the DNA solutions and incubated at 37 °C for 1 h. The fluorescence emission was monitored from 452 nm to 650 nm, with an excitation wavelength of 442 nm.

3.7 References

(1) Zheng, J.; Yang, R.; Shi, M.; Wu, C.; Fang, X.; Li, Y.; Li, J.; Tan, W. *Chem. Soc. Rev.* **2015**, *44* (10), 3036–3055.

(2) Tyagi, S.; Kramer, F. R. *Nat. Biotechnol.* **1996**, *14* (3), 303–308.

(3) Bratu, D. P.; Cha, B.-J.; Mhlanga, M. M.; Kramer, F. R.; Tyagi, S. *Proc. Natl. Acad. Sci.* **2003**, *100* (23), 13308–13313.

(4) Tang, Z.; Wang, K.; Tan, W.; Ma, C.; Li, J.; Liu, L.; Guo, Q.; Meng, X. *Nucleic Acids Res.* **2005**, *33* (11), e97–e97.

(5) Wu, C.; Chen, T.; Han, D.; You, M.; Peng, L.; Cansiz, S.; Zhu, G.; Li, C.; Xiong, X.; Jimenez, E.; et al. *ACS Nano* **2013**, *7* (7), 5724–5731.

(6) Chen, T.; Wu, C. S.; Jimenez, E.; Zhu, Z.; Dajac, J. G.; You, M.; Han, D.; Zhang, X.; Tan, W. *Angew. Chem. Int. Ed.* **2013**, *52* (7), 2012–2016.

(7) Ellington, A. D.; Szostak, J. W. *Nature* **1990**, *346* (6287), 818–822.

(8) Tuerk, C.; Gold, L. *Science* **1990**, *249* (4968), 505–510.

(9) Li, J. J.; Fang, X.; Tan, W. *Biochem. Biophys. Res. Commun.* **2002**, *292* (1), 31–40.

(10) Hamaguchi, N.; Ellington, A.; Stanton, M. *Anal. Biochem.* **2001**, *294* (2), 126–131.

(11) Stojanovic, M. N.; de Prada, P.; Landry, D. W. *J. Am. Chem. Soc.* **2001**, *123* (21), 4928–4931.

(12) Fang, X.; Sen, A.; Vicens, M.; Tan, W. *ChemBioChem* **2003**, *4* (9), 829–834.

(13) Yamamoto, R.; Kumar, P. K. R. *Genes Cells* **2000**, *5* (5), 389–396.

(14) Nutiu, R.; Li, Y. *J. Am. Chem. Soc.* **2003**, *125* (16), 4771–4778.

(15) Fu, R.; Li, T.; Lee, S. S.; Park, H. G. *Anal. Chem.* **2011**, *83* (2), 494–500.

(16) Li, D.; Shlyahovsky, B.; Elbaz, J.; Willner, I. *J. Am. Chem. Soc.* **2007**, *129* (18), 5804–5805.

(17) Xiao, Y.; Pavlov, V.; Niazov, T.; Dishon, A.; Kotler, M.; Willner, I. *J. Am. Chem. Soc.* **2004**, *126* (24), 7430–7431.

(18) Gao, W.; Zhang, L.; Zhang, Y.-M.; Liang, R.-P.; Qiu, J.-D. *J. Phys. Chem. C* **2014**, *118* (26), 14410–14417.

(19) Teller, C.; Shimron, S.; Willner, I. *Anal. Chem.* **2009**, *81* (21), 9114–9119.

(20) Knowles, J. R. *Annu. Rev. Biochem.* **1980**, *49* (1), 877–919.

(21) Huizenga, D. E.; Szostak, J. W. *Biochemistry* **1995**, *34* (2), 656–665.
(22) Ma, C.; Lin, C.; Wang, Y.; Chen, X. *Trends Anal. Chem.* **2016**, *77*, 226–241.
(23) Liu, J.; Lu, Y. *Angew. Chem. Int. Ed.* **2006**, *45* (1), 90–94.
(24) Wang, J.; Wang, L.; Liu, X.; Liang, Z.; Song, S.; Li, W.; Li, G.; Fan, C. *Adv. Mater.* **2007**, *19* (22), 3943–3946.
(25) Zuo, X.; Song, S.; Zhang, J.; Pan, D.; Wang, L.; Fan, C. *J. Am. Chem. Soc.* **2007**, *129* (5), 1042–1043.
(26) Zuo, X.; Xiao, Y.; Plaxco, K. W. *J. Am. Chem. Soc.* **2009**, *131* (20), 6944–6945.
(27) Wang, L.; Xu, M.; Han, L.; Zhou, M.; Zhu, C.; Dong, S. *Anal. Chem.* **2012**, *84* (17), 7301–7307.
(28) Xing, Y.; Yang, Z.; Liu, D. *Angew. Chem. Int. Ed.* **2011**, *50* (50), 11934–11936.
(29) Stojanovic, M. N.; Kolpashchikov, D. M. *J. Am. Chem. Soc.* **2004**, *126* (30), 9266–9270.
(30) Wang, J.; Jiang, Y.; Zhou, C.; Fang, X. *Anal. Chem.* **2005**, *77* (11), 3542–3546.
(31) He, H.-Z.; Pui-Yan Ma, V.; Leung, K.-H.; Shiu-Hin Chan, D.; Yang, H.; Cheng, Z.; Leung, C.-H.; Ma, D.-L. *Analyst* **2012**, *137* (7), 1538.
(32) Wang, H.; Peng, P.; Liu, S.; Li, T. *Anal. Bioanal. Chem.* **2016**, *408* (28), 7927–7934.
(33) Zheng, D.; Seferos, D. S.; Giljohann, D. A.; Patel, P. C.; Mirkin, C. A. *Nano Lett.* **2009**, *9* (9), 3258–3261.
(34) Prigodich, A. E.; Seferos, D. S.; Massich, M. D.; Giljohann, D. A.; Lane, B. C.; Mirkin, C. A. *ACS Nano* **2009**, *3* (8), 2147–2152.
(35) Li, N.; Chang, C.; Pan, W.; Tang, B. *Angew. Chem. Int. Ed.* **2012**, *51* (30), 7426–7430.
(36) Özalp, V. C.; Schäfer, T. *Chem. Eur. J.* **2011**, *17* (36), 9893–9896.
(37) Takeda, S.; Miyauchi, S.; Nakayama, H.; Kamo, N. *Biophys. Chem.* **1997**, *69*, 175–183.
(38) Bauer, M.; Baumann, J.; Trommer, W. E. *FEBS Lett.* **1992**, *313* (3), 288–290.